Cellulose (2025) 32:919–940
https://doi.org/10.1007/s10570-024-06341-6

ORIGINAL RESEARCH

Green synthesis and optimization of selenium nanoparticles using chitosan or cationic cellulose nanofibers

Samanta Sam · Nuria Fiol · Roberto J. Aguado · Elena Saguer · Félix Carrasco · Marc Delgado-Aguilar · Quim Tarrés

Received: 13 September 2024 / Accepted: 13 December 2024 / Published online: 23 December 2024

Abstract Spherical selenium nanoparticles (Se NPs) were synthesized by green chemical reduction method using biocompatible chitosan (CS) or as reported herein for the first time, cationic cellulose nanofibers (CCNFs) as stabilizers. CNFs were cationized using (3-chloro-2-hydroxypropyl) trimethylammonium chloride (CHPTAC), followed by high-pressure homogenization. The anionic demand of the CCNFs was found to be 2000 ± 2 µeq/g and the degree of substitution was 0.25 ± 0.01. The optimization of Se NP synthesis was done using response surface methodology with controlled composite design. Two response surface models were developed to optimize the size and stability of CS-Se NPs and CCNF-Se NPs. Concentrations of Na_2SeO_3, ascorbic acid, and CS or CCNFs were used as three variables, and their interaction was studied as a function of size and zeta potential. The results indicate that the variables fitted into the model and was validated using a combined contour plot of size and zeta potential. From the model, CS-Se NPs of size and zeta potential in the range between 10 and 70 nm and 30–40 mV were synthesized, while CCNF-Se NPs of size and zeta potential in the range between 50 and 85 nm and 30–35 mV were synthesized. EDX spectra confirmed elemental Se formation, and XRD pattern verified the presence of α-monoclinic Se crystallites. Additionally, the FTIR spectra confirmed the interaction between the stabilizing agent and Se NPs. Thus, CS- and CCNF-stabilized Se NPs were sustainably synthesized making them suitable for incorporation into CNFs and can be used as an active agent in food packaging application.

Supplementary Information The online version contains supplementary material available at https://doi.org/10.1007/s10570-024-06341-6.

S. Sam · N. Fiol · R. J. Aguado · E. Saguer · F. Carrasco · M. Delgado-Aguilar · Q. Tarrés (✉)
LEPAMAP-PRODIS Research Group, University of Girona, C/ Maria Aurèlia Capmany, 61, 17003 Girona, Spain
e-mail: joaquimagusti.tarres@udg.edu

Graphic abstract

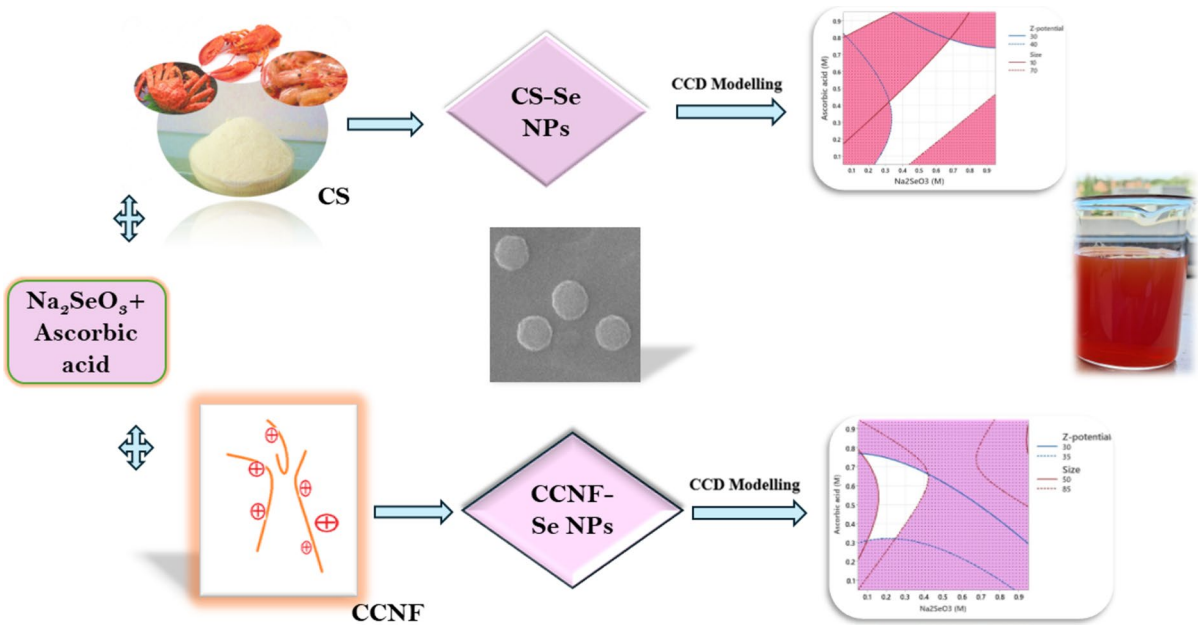

Keywords Chitosan · Cationic cellulose nanofibers · Cellulose · Selenium · Nanoparticle · Response surface methodology

Introduction

Selenium (Se) is a crucial trace element in human physiology, significantly contributing to health and growth (Luo et al. 2020; Ndwandwe et al. 2021). Se is a major component of selenoenzymes, which protect animal cells from oxidative stress and has been extensively studied for its antioxidant activity. It is well-documented that Se possesses unique properties distinguishing it from other metals and metalloids. Researchers have chosen selenium for various reasons, particularly because of its applications in ecological, ecotoxicological, and radioecological sciences (Kapur et al. 2017). Nanotechnology is a rapidly evolving field focused on the development of innovative materials (Vankudoth et al. 2022; Ran et al. 2024). Particles with dimensions from 1 to 100 nm are known as nanoparticles (Prasad et al. 2017). Many scientists predict that nanotechnology will drive the next industrial revolution, significantly influencing society, the economy, and daily life (Hashem, Al-Askar, Haponiuk, et al. 2023). Recently, Se NPs have garnered increasing attention due to their high biocompatibility (Skalickova et al. 2017), antioxidant activities (Hu et al. 2021), low toxicity (Shakibaie et al. 2013), antimicrobial activity (Hashem, Al-Askar, Saeb, et al. 2023) and unique therapeutic properties (Xiao et al. 2023). Se NPs were found to show potential application because of their minimal toxicological effect and increased bioavailability along with their exceptional biocidal effect compared to other forms of selenium, such as selenate (SeO_4^{2-}) and selenite (SeO_3^{2-}) (Fatma et al. 2019). Nano Se, which is bright orange-red color in the oxidation state of Se (0), is emerging as a novel source of selenium in the fields of food and pharmaceutical sciences (Hosnedlova et al. 2018).

Various approaches, including physical, biological, and chemical processes (Kumar et al. 2021; Liu et al. 2022), are used for the synthesis of nanoparticles (Modrzejewska-Sikorska et al. 2017; Bisht et al. 2022). The wide use of these metal/metal oxide nanoparticles are due to their ease of synthesis and large surface area (Rasool et al. 2023). Chemical

wet processing is considered to be the most facile and effective method among all the others since it involves the use of reducing agents to convert metallic salts into zero-valent metals, followed by capping and stabilizing the nanoparticles with surfactants and organic polymers (Sarwar et al. 2021). Reducing agents and capping agents play a major role in nanoparticle synthesis as the nanoparticle's characteristics are influenced by them. Surfactants or reagents such as polyvinyl chloride (PVC) (Wang et al. 2013), polyvinyl alcohol (PVA) (Al Jahdaly et al. 2021) are used for the stabilizing effect in nanoparticles synthesis, but they are sourced from the petrochemical industry. Likewise, a well-known and ubiquitous reducing agent, sodium borohydride, succeeds at quickly attaining NPs, but its biological hazards make it inadequate, *e.g.*, for applications involving food contact (Xiong et al. 2011). Here comes the role of green synthesis as it is an optimal method for preparing nanoparticles, offering significant advantages such as reduced toxicity, increased stability, eco-friendliness, and cost-effectiveness (Akram et al. 2024). These methods are particularly beneficial for environmental and biomedical applications, providing a more sustainable and safe approach compared to traditional techniques (Vijayaram et al. 2024). These include synthesis using bacteria or plant extracts (Pyrzynska and Sentkowska 2022; Zhai et al. 2024), microwave synthesis (Panahi-Kalamuei et al. 2014), and electrochemical methods (Ye et al. 2017). These can be expensive or may not produce the desired products. Solution-phase chemical reduction methods offer an excellent route for fabricating selenium nanoparticles, despite the availability of various conventional techniques for their synthesis (Zhang et al. 2004). The most commonly used reducing agent in green synthesis of metal NPs is ascorbic acid because it allows the reaction to be performed at ambient temperature in water, besides being affordable and non-toxic (Štefanková et al. 2023).

Moreover, chitosan and cellulose nanofibers have excellent biocompatible properties and can be used as stabilizers in nanoparticles synthesis. Chitosan (CS) is a well-characterized, biodegradable, biocompatible, hydrophilic, nonimmunogenic, non-toxic, and cost-effective polymer and find a wide range of application in food, agriculture, and biotechnology (Negm et al. 2020; Abdelhamid et al. 2024). It is extracted from the exoskeletons of arthropods and the cell walls of fungi and can also be synthetically produced by the deacetylation of chitin. It is found to be a good stabilizer in the synthesis of nanoparticles in several studies (Zeng et al. 2018). Another most abundant biopolymer available on earth is cellulose, which is composed of β-1,4 linked glycosidic units (Peng et al. 2019). On the other hand, cellulose nanofibers (CNFs) are garnering significant attention since they exhibit high surface ratio, low toxicity, and are renewable (Ahmadi et al. 2021). They have been incorporated as a stabilizer in the nanoparticles synthesis (Chen et al. 2022). Surface functionalized CNFs have been used as a stabilizer in the synthesis of silver nanoparticles (Jang et al. 2014; Islam et al. 2018). They can be surface functionalized using different cationic and anionic reagents (Harper et al. 2016). These techniques primarily utilize the abundance of hydroxyl groups on the surface, enabling the straightforward conjugation of desired molecules. As far as the authors are concerned, there is no previous study using CCNFs as a stabilizer in Se NP synthesis. In the case of CCNFs, it leverages the electrostatic interactions between cationically modified cellulose surfaces and negatively charged metal nanoparticles or metal complex ions and play as a capping or a stabilizing agent for the negatively charged Se NPs. They can be applied to both porous and nonporous cellulose fibers. Thus, the negatively charged metal nanoparticles get deposited on the cationically modified cellulose substrate thus enabling stable nanoparticle suspension. The cationization was done using (3-chloro-2-hydroxypropyl) trimethylammonium chloride (CHPTAC) and this introduces quaternary ammonium groups on the surface of CNFs. It was reported that these cationic moieties have intrinsic antibacterial properties (Pedrosa et al. 2022). Cationic cellulose nanofibrils have a high aspect ratio, large specific surface area, strong biocompatibility, excellent biodegradability, and superior mechanical strength, offering a renewable and sustainable alternative to petroleum-based cationic nanomaterials in textiles, papermaking, packaging, and wastewater treatment applications (Long et al. 2024).

In order to reduce the time and cost, it is necessary to optimize the size and stability of the nanoparticles synthesized. Traditional one-variable optimization overlooks interactions, lacks comprehensive understanding, and increases experiments, costs, and research time. Here comes the role of response surface methodology (RSM) in resolving these kinds of problems.

RSM is a foremost multivariate statistical technique extensively applied in optimizing experimental conditions, particularly in food processes. RSM comprises a suite of statistical and mathematical methods rooted in fitting polynomial models to data, aiming to portray dataset behavior for statistical predictions (Saylam et al. 2021). This approach proves invaluable in optimizing, designing, developing, and enhancing processes where multiple variables influence one or more responses (Yolmeh and Jafari 2017). Before applying the RSM approach, it is essential to select the appropriate experimental design to determine which treatments should be conducted within the experimental region under study. Achieving Se NPs with the desired size and stability necessitates optimizing the synthesis factors through design of experiments (DOE) (Lalegani and Seyyed Ebrahimi 2020). It is a collection of valuable mathematical techniques applied to the statistical modeling and systematic analysis of problems where input variables or factors are used to optimize desired responses or output measures (Tsimpliaraki et al. 2009). Examples of experimental designs include Central Composite, Box-Behnken, and Doehlert designs. The Box-Wilson second-order central composite design (CCD) is gaining popularity as it optimally assigns operational variables for evaluations, using a rational number of design points and providing reliable curvature estimation, ensuring sufficient information for lack-of-fit testing (Ghelich et al. 2019).

This work involves the synthesis and optimization of Se NPs using two bio-based stabilizing and capping agents: CCNFs, not used before for this purpose, and CS. The other key contribution lies in the optimization strategy by response surface methodology (RSM). Two parallel methods were employed, one with chitosan and the other with CCNFs. The optimization of both CS-Se NPs and CCNF-Se NPs was conducted using RSM methodology. In this study, Se NPs were prepared via a green, low-cost chemical reduction method using Na_2SeO_3 as the metal precursor, with CS and CCNFs as stabilizers, and L-ascorbic acid as the reducing agent. Data analysis was performed using DOE, and two response surface models were derived to optimize the size and stability of the synthesized Se NPs using CCD modeling. Ultraviolet–Visible (UV–Vis) spectrophotometry was employed as a preliminary characterization technique to confirm the formation of Se NPs, followed by Dynamic Light Scattering (DLS) to measure particle size based on Brownian motion and the zeta potential (as stability measurement) of CS- and CCNF-stabilized Se NPs. Characterization techniques such as determination of anionic demand, degree of substitution, quantification of hemicellulose and nano fibrillation yield of the CCNFs was tested. Field Emission Scanning Electron Microscopy (FESEM) in conjunction with Energy Dispersive X-ray (EDX) microanalysis and X-ray diffraction (XRD) experiments were conducted to determine the morphology (size and shape) and elemental composition of the synthesized Se NPs. Fourier Transform Infrared (FTIR) spectroscopy was used to confirm the Se NPs interaction with the stabilizers. The optimization of Se NP synthesis using CCD aims to develop applications in active food packaging. Thus, this work demonstrates the sustainable synthesis of Se NPs, and this can be further used as an antioxidant agent in the active food packaging application.

Experimental section

Materials

All the chemicals and reagents were of analytical grade and used without further purification. Sodium selenite (Na_2SeO_3) anhydrous, 99% (metal basis) was purchased from Thermo-Scientific (Cornellà, Spanish branch office). CS with molecular weight in the 50–190 kDa range and with a deacetylation degree of 99% was purchased from Sigma-Aldrich (Barcelona, Spanish branch office), and so was L-Ascorbic acid with molecular weight 176.12 g/mol. ($C_6H_8O_6$).

The starting material for the production of CCNFs was bleached kraft eucalyptus pulp from industrial origin. The high-pressure homogenizer implied in this production was the PANDA 2 K-GEA, model NS1001L (GEA Niro Soavy, Parma, Italy). The water used throughout the experimental procedure was ultrapure Milli-Q water.

Production of cationic cellulose nanofibers (CCNFs)

Cationization of CNFs, preceded by PFI refining and alkalization, was performed as described by Giovana et. al (Signori-Iamin et al. 2024). In brief, CCNFs were prepared from the mechanical refining of disintegrated bleached kraft eucalyptus pulp at 15,000 PFI revolutions and was mercerized with NaOH, then

cationized with 3-chloro-2-hydroxypropyl trimethylammonium chloride. The reaction was carried out at 60 °C, with molar excess of cationizing agent, and without a filtration step between alkalization and cationization. The pulp was then suspended at distilled water at 1 wt.% and the above solution was passed through the homogenizer at 3 passes each at 300 bar, 600 bar and 900 bar.

Selenium nanoparticle synthesis using chitosan (CS-Se NPs) and cationic cellulose nanofibers (CCNF-Se NPs) as stabilizers

Se NPs using CS and CCNFs were prepared in the same way. 1 mL of Na_2SeO_3 (metal precursor) was added dropwise with continuous stirring to the solution containing 100 mL of ascorbic acid (reducing agent) and chitosan or CCNFs (stabilizer and capping agent) drop by drop within 35 min and stirred again the whole solution for about 15 min. It was observed that the color changes from colorless to orange-red upon each drop added. This color change indicates the formation of Se NPs as all the reagents used in the reaction were colorless. The synthesized NPs were then stored at 4 °C for further analysis. Se NPs synthesized using the two different stabilizers exhibited almost similar color which is a dark orange-red color.

Characterization techniques

Ion chromatography

The quantification of the remaining hemicellulose was performed using ion chromatography to identify the various monosaccharides present after acid hydrolysis. The hydrolysis followed the two-step procedure outlined in NREL/TP-510–42618 (Sluiter et al. 2008). Initially, a sample of cationized cellulose nanofibers was subjected to depolymerization using 72 wt% aqueous H_2SO_4 at 30° C for 1 h. Subsequently, the mixture was diluted to a concentration of 4 wt% H_2SO_4 and autoclaved at 121° C for 1 h. The resulting hydrolysate was then analyzed using a Dionex ICS-5000 DP chromatograph (Sunnyvale, CA, USA) equipped with an anion exchange column and an amperometric detector.

Conductometric titration

The degree of substitution (DS) for cationic fibers was determined through conductometric titration of chloride counter-ions, based on the principle that each trimethylammonium group associates with one counter-ion, following the method outlined by Pei et al. (2013) and Rol et al. (2019) (Pei et al. 2013; Rol et al. 2019). Initially, 0.4 g of dry fiber was mixed with 200 mL of distilled water. Conductometric titration was then carried out by incrementally adding 0.2 mL of a 0.06 M silver nitrate ($AgNO_3$) solution every 30 s to the mixture. The DS was calculated using the following equation:

$$DS = \frac{n_{AgNO3}}{n_{cellulose}} = \frac{C_{AgNO3} * V_{AgNO3}}{\frac{m_{cellulose}}{M_{AGU}}} \quad (1)$$

where C_{AgNO3} is the molar concentration, V_{AgNO3} is the volume of $AgNO_3$ solution used to reach equivalence, $m_{cellulose}$ is the dry weight of cellulose, and M_{AGU} is the molar mass of an anhydroglucose unit (162 g/mol).

Potentiometric titration

The anionic demand of cationic cellulose nanofibers was assessed through potentiometric back titration (Serra-Parareda et al. 2021) using a Mütek PCD-06 particle charge analyzer (BTG Instruments, Wessling, Germany). In summary, 0.02 g of dry sample was soaked in an excess amount of sodium polyethylene sulfonate (PES-Na, 0.001 mol/L). Following this, the sample was centrifuged at 2,300 g for 20 min, and 10 mL of the supernatant was titrated with a 0.001 mol/L solution of polydiallyldimethylammonium chloride (polyDADMAC).

UV–Vis spectrophotometry

A Shimadzu UV-1280 spectrophotometer (Duisburg, European branch office) in the wavelength range 200–800 nm was used to measure the UV–Vis spectra of the synthesized CS-Se NPs and CCNF-Se NPs. It was done to confirm their formation from their characteristic surface plasmon resonance (SPR) band. Milli-Q water was used as the background. Absorbance measurements were taken from 1:100 dilutions of Se NP solutions at room temperature.

Dynamic light scattering measurement (DLS)

The mean particle size of CS-Se NPs and CCNF-Se NPs was determined by DLS using the Zetasizer Nano ZS device (Malvern Instruments, Malvern, United Kingdom), which employs the Mie theory and the Stokes–Einstein relation (Kapur et al. 2017). For that, 1 mL of the prepared Se NP dispersion was diluted to 100 mL and the measurements were taken using a polystyrene cuvette with 3 × 3 mm, 5 × 5 mm or 10 × 10 mm dimension at 25 °C. The zeta potential was directly measured from the synthesized Se NP dispersion using the same instrument, but with cuvettes comprising gold electrodes.

Fourier transform infrared spectroscopy (FT-IR)

Fourier Transform Infrared (FT-IR) spectra was recorded on Bruker Alpha FT-IR spectrophotometer (Karlsruhe, Germany) with a resolution of 2 cm^{-1} to identify the functional groups and the interaction between Se NPs with chitosan, CCNFs, and other reagents used in NP synthesis. The suspensions of synthesized CS-Se NPs and CCNF-Se NPs were dried and ground to homogenous powder, before mounted on a diamond crystal plate ATR MIR single-reflection accessory and scanned at a wavenumber range from 400–4000 cm^{-1}. Analysis of spectra was performed using OPUS_7.5.18 software.

Field emission scattering electron microscopy (FESEM)

A TESCAN Clara (Brno-Kohoutovice, Czech Republic) field-emission scanning electron microscope was used to obtain FESEM images of the synthesized CS-Se NPs and CCNF-Se NPs to determine their size and shape. The images were taken in high vacuum and at an accelerating voltage of 15 kV.

Energy dispersive X-ray spectroscopy (Edx)

EDX spectroscopy was used in conjunction with the FESEM instrument at high vacuum, 20 kV to determine the elemental composition of the samples. EDX spectra of CS-Se NPs and CCNF-Se NPs were measured in conjunction with FESEM. The atom percentage of metal in EDX analysis aids in determining the sample's purity and elemental composition.

X-ray diffraction analysis (XRD)

X-ray diffraction analysis (XRD) was used to distinguish the crystalline allotropes in Se NPs, employing a Brucker AXS D8 Advance powder diffractometer (Karlsruhe, Germany). Measurements were done from 5° to 100° using Bragg–Brentano (θ, 2θ) geometry and the reflection mode, involving Cu Kα radiation from an X-Ray tube with a wavelength of 1.5418 Å. The scanning speed and step length were 0.05° and 1 s, respectively. A secondary graphite monochromator and a scintillation NaI (Tl) point detector were included.

Experimental design and statistical analysis for optimization of size and stability

Response Surface Methodology (RSM) was used to optimize the size and stability of the Se NPs. Contour plot, surface plots and main effect graphs for size and zeta potential were plotted using Minitab statistical software (Pennsylvania, USA). Different concentrations of ascorbic acid, Na_2SeO_3, and CS or CCNFs were used as the independent variables and were plotted as a function of size and zeta potential. A face-centered central composite design (CCD) was used to perform the response surface methodology for the optimization of Se NP synthesis in our present work. CCD is a fractional factorial design with center points, augmented by a set of axial points. Accordingly, 15 experimental combinations were randomly tested for each experiment set with the aid of Minitab statistical software. In these 15 points, the first 9 points are known as factorial points and the subsequent 5 points are known as axial points and remaining last one is known as center point. These 15 sets were derived from the Eq. 2:

$$N = 2^K + 2k + n_c \quad (2)$$

where the number of factors (k) is 3, namely Na_2SeO_3, chitosan or CCNFs, and ascorbic acid; n_c is the number of central points, *i.e.* 1 since we keep one variable constant while changing the other two variables. Na_2SeO_3 and ascorbic acid concentrations ranged from 0.05 M to 0.95 M, while CS and CCNF concentrations varied between 1 and 2% and between 0.05 and 1 wt%, respectively. The concentrations were selected based on previous experiments. The

model equation was formulated in terms of a multiple regression analysis. Its coefficients and their significance were estimated by means of Minitab Statistical Software, choosing a stepwise procedure with backward elimination. Significant coefficients resulted from fitting the experimental data to a second-order polynomial equation (Eq. 3):

$$Y = b_0 + \sum_{i} = 1^{n} b_i X_i + \sum_{\substack{i=1 \\ j>1}}^{n-1} \sum_{j=2}^{n} b_{ij} X_i X_j + \sum_{i=1}^{n} b_{ii} X_i^2 \quad (3)$$

Table 1 CCD matrix of different combinations of three independent variables

Run	Na_2SeO_3 (M)	Ascorbic acid(M)	Chitosan(%)	CCNF(%wt)
1	0.5	0.5	1.5	–
2	0.05	0.05	1	–
3	0.05	0.95	1	–
4	0.05	0.05	2	–
5	0.05	0.95	2	–
6	0.95	0.05	1	–
7	0.95	0.95	1	–
8	0.95	0.05	2	–
9	0.95	0.95	2	–
10	0.05	0.5	1.5	–
11	0.95	0.5	1.5	–
12	0.5	0.5	1	–
13	0.5	0.5	2	–
14	0.5	0.05	1.5	–
15	0.5	0.95	1.5	–
16	0.5	0.5	–	0.525
17	0.05	0.05	–	0.05
18	0.05	0.95	–	0.05
19	0.05	0.05	–	1
20	0.05	0.95	–	1
21	0.95	0.05	–	0.05
22	0.95	0.95	–	0.05
23	0.95	0.05	–	1
24	0.95	0.95	–	1
25	0.05	0.5	–	0.525
26	0.95	0.5	–	0.525
27	0.5	0.5	–	0.05
28	0.5	0.5	–	1
29	0.5	0.05	–	0.525
30	0.5	0.95	–	0.525

where Y represents the response size and zeta potential to be modelled; b_0 is the constant coefficient (value of the fixed response at the centre point of the design), b_i is the coefficient of linear effect, b_{ij} is the coefficient of interaction effect, b_{ii} the coefficients of squared-effect, n is the number of variables and X_i and X_j define the independent variables (concentration of Na_2SeO_3, ascorbic acid, chitosan, and CCNFs) (Amado et al. 2014). The data in Table 1 were used in the Minitab statistical software to derive the regression equation and in the design of the main effect plot, three-dimensional surface graphs, and the two-dimensional contour plots which are detailed in the results and discussion section.

Results and discussion

Characterization of CCNFs

The degree of substitution of the CCNFs, determined by titration of chloride counter-ions, was 0.25 ± 0.01. Furthermore, the hydrolysate of the CCNFs was found to contain 87.85 wt% glucose and 12.01 wt% xylose, with arabinose, mannose, and glucuronic acids below the detection limit, indicating no excessive damage to the fibers and preserved hemicelluloses. The anionic demand (charge density) of CCNFs was 2.0 ± 0.2 meq/g (Signori-Iamin et al. 2024). Additionally, the nano fibrillation yield was found to be greater than 95%. As the fibrillation process increases, the surface area increases as there is an increased exposure to the quaternary ammonium groups because of the cationization and it has a high content of nanofibers. An image of the synthesized CCNFs is shown in Fig. 1S (Supplementary material). It can act as a capping or stabilizing agent with the negatively charged Se NPs. They can cap the Se NPs by electrostatic interactions thus providing stability to the medium and generating a homogeneous suspension.

Qualitative analysis of stabilizing agents in the Se NP formation

Initially, to evidence the effect of stabilizing agents (CS or CCNFs) on the formation of Se NPs, Na_2SeO_3 was added to a solution containing ascorbic acid and

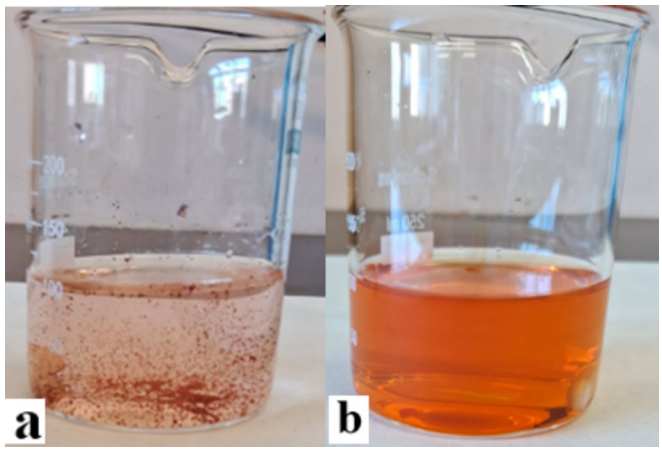

Fig. 1 Effect of stabilizing agents on the Se NP formation: **a** the solution without stabilizing agent, **b** the solution with stabilizing agent (CS or CCNFs)

CS or CCNFs, with the concentrations of each reagent varying depending on the stabilizing agent. Figure 1 illustrates the notable effect of a stabilizing agent on the formation and stability of Se NPs in solution. In the absence of any stabilizers such as CS or CCNFs, the Se particles exhibited pronounced aggregation (Fig. 1a). This aggregation resulted in the formation of macro-sized particles that settled at the bottom of the container, indicating poor stability and homogeneity in the solution. One mL of (0.7 M or 0.3 M) Na_2SeO_3 was added to the solution containing 100 mL of (0.7 M or 0.5 M) ascorbic acid and 1.8% of CS or 0.3% wt of CCNFs, respectively. 0.7 M Na_2SeO_3 and ascorbic acid was in the case of CS-Se NP synthesis whereas the concentration was 0.3 M and 0.5 M for Na_2SeO_3 and ascorbic acid, respectively, for the CCNF-Se NP synthesis. Both of them showed similar colour change and stabilizing effect, which is shown in Fig. 1. The introduction of stabilizing agents led to a successful reduction in the nanoscale dimensions of Se particles. This change was visually evident as the solution became uniformly dispersed, with no visible settling or aggregation of particles (Fig. 1b).

CS contributed to Se NP stabilization through its ability to provide steric hindrance and electrostatic repulsion (Luesakul et al. 2016). Its positive charge in an acidic medium can interact with the negatively charged surface of Se NPs, preventing close contact between Se NPs and thus preventing their aggregation. This electrostatic stabilization is crucial in maintaining the colloidal stability of nanoparticles. Similarly, CCNFs offer stabilization through its high aspect ratio and large specific surface, which can adsorb selenium nanoparticles (Dong and Hinestroza 2009). The CCNFs network provides a mechanical barrier that effectively prevents particle aggregation. Additionally, the cationic groups incorporated into the cellulose nanofiber surface during the cationization process with CHPTAC further inhibit particle aggregation.

Table 2 Determination of Se NPs size and zeta potential at different chitosan concentrations

Sample no	Size (nm)		Zeta potential (mV)	
	Mean	SD	Mean	SD
1	17.8	4.6	36.5	0.2
2	34.0	3.7	46.8	0.6
3	37.2	0.4	39.7	1.8
4	31.4	6.6	38.9	0.3
5	37.8	17.1	34.0	0.6
6	161.0	3.3	31.1	0.8
7	42.9	0.6	28.1	0.2
8	206.0	5.0	32.8	0.2
9	27.7	15.1	28.6	0.3
10	15.3	3.9	49.4	1.0
11	23.6	3.4	35.2	0.6
12	37.2	2.4	36.0	1.0
13	19.4	4.4	37.6	0.6
14	46.1	2.9	38.3	0.2
15	18.0	2.7	30.5	1.4

RSM model for the optimization of size and zeta potential of CS-Se NPs

CCD was used to determine the effect of 3 explanatory variables selected on size and zeta potential of the synthesized Se NPs. Table 2 shows the results obtained for each of the 15 tested formulations using CS as a stabilizing agent.

As observed in Table 2, the particle size of Se NPs synthesized under different conditions using CS as a stabilizing agent varies notably, ranging from 15 to 206 nm. This wide range of sizes demonstrates the possibility to control particle size, achieving even extremely small sizes. In particular, a combination of 1.5 wt % CS with a solution of 0.05 M Na_2SeO_3 and 0.5 M ascorbic acid produced Se NPs with a size as low as 15.35 nm. This ability to achieve such small sizes is crucial for applications requiring high specific surface area and unique properties at the nanoscale (Khan et al. 2019). Furthermore, the zeta potential, which indicates the stability of the nanoparticles and consequently their no aggregation, ranged between 28 and 50 mV.

The standardized effects of the independent variables and their interaction on the responses can be better visualized using Pareto chart. The length of each bar in the chart indicates the standardized effect of the factor on the responses. In this case, the factors selected here are the reagents used in this reaction and the responses are size and zeta potential. The bars corresponding to each factor protruding outside the reference line (which is marked as 1.559 in Fig. 2a and 2b) contribute more to the prediction of the particle size and zeta potential. In Fig. 2, the three factors were named A, B, C corresponding to concentrations of Na_2SeO_3, chitosan, and ascorbic acid, respectively. Specifically, in the case of CS-Se NPs, it was found that the concentration of Na_2SeO_3 (A) and ascorbic acid (C), that is the metal precursor and the reducing agent, respectively, have a significant effect on the variation in values of the responses (size and zeta potential).

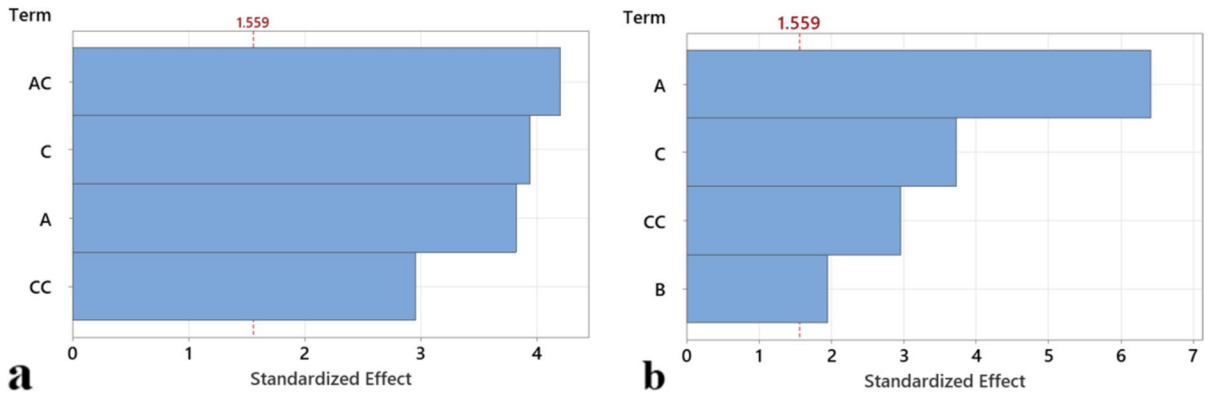

Fig. 2 **a** Pareto chart for size; **b** Pareto chart for zeta potential of CS-Se NPs

Table 3 Analysis of variance of size and zeta potential of CS-Se NPs using the backward method

Analysis of Variance (Significant Values)	Size		Zeta potential	
	F-Value	P-Value	F-Value	P-Value
Model	14.13	0.000	16.88	0.000
Na_2SeO_3	14.63	0.003	41.15	0.000
Chitosan	Neglected		3.77	0.081
Ascorbic acid	15.52	0.003	13.84	0.004
Chitosan*Chitosan	Neglected		Neglected	
Ascorbic acid*Ascorbic acid	8.73	0.014	8.76	0.014
Na_2SeO_3*Ascorbic acid	17.64	0.002	Neglected	

The above observation can also be confirmed by the F-value from the Table 3 of analysis of variance. The significance of the effect of the concentration of respective variables and their interaction on the considered responses can be evaluated from the F-value.

The global Fischer's F-test values of 14.13 for size and 16.88 for stability indicate that the model is significant. The only probability for the F-value to be this large is only 0.01%. In the analysis of the variance table, the highest F-values were observed for Na_2SeO_3 (A) and ascorbic acid (C), hence proving their major contribution or effect in varying the size and stability of CS-Se NPs. The only interaction that was deemed significant to size was the one between A and C. Hence, they cannot be considered to exert independent effects over nanoparticle size. In the case of zeta potential, no interaction was deemed significant, leaving all individual factors as independent variables.

Additionally, the p-value has also an effect on determining the significance of the model, *i.e.,* the terms with corresponding p-values smaller than 0.05 were considered significant in their impact on the response. The p-values of the model for size and stability were 0.000 and 0.000, respectively, which indicates that the model is statistically significant. The p-values for A (Na_2SeO_3) and C (ascorbic acid) for zeta potential of CS-Se NPs indicate their major contribution in the reaction and the statistical significance of the model. The coefficient of determination (R^2) value for the size of CS-Se NPs from the statistical report of the model summary was 0.85, while the R^2 value for zeta potential was 0.87, which indicates that the variables fitted into the model. This means that 85% and 87% of the variation in the size and zeta potential of the NPs was due to the change in the concentration of three variables. These values were close to 1 and it indicates a strong agreement between the experimental data and the model-predicted results. The model could be represented as Eq. 4 and 5 which are the regression equation in uncoded units for size and zeta potential for CS-Se NPs, where A-Na_2SeO_3, B-Chitosan, C-Ascorbic acid. This equation represents the interaction of the factors between themselves and with others. The regression coefficient's magnitude reflects the potency of the different terms within the model.

$$\text{Size} = 27.9 + 162.1A - 181.0C + 203.9C * C - 187.0A * C \quad (4)$$

$$\text{Zeta potential} = 49.34 - 13.78A - 3.75B + 16.49C + 24.48C * C \quad (5)$$

To better understand the effects of independent variables and their interactions on the response, as well as the conditions yielding the optimum values for both responses, the experimental conditions were further analyzed. This was done by constructing three-dimensional response surface graphs and two-dimensional contour plots derived from regression Eqs. 4 and 5.

In the case of CS-Se NPs, the concentration of CS was held at 1.5 wt% as it doesn't have much influence in the variation of Se NPs size and stability. The nonlinear nature of all the three-dimensional response surfaces indicates significant interactions between the independent variables, showing that they had mutually dependent influences on the responses. The main effect plot of CS-Se NPs is shown in Fig. 2 Sa and 1 Sb (Supplementary material) which illustrates the distribution of size and zeta potential at various concentrations of the reagents (Fig. 3).

The data presented in all the plots indicate the successful synthesis of CS-Se NPs with small size and high stability. The stability of the nanoparticles is inferred from the zeta potential values, with higher zeta potential indicating greater stability. From the graphs, it is evident that the synthesized CS-Se NPs have sizes ranging from 10 to 70 nm and zeta potential values between 30 and 40 mV. These results were achieved when the concentration of Na_2SeO_3 and ascorbic acid were between 0.5 M and 0.95 M, and the concentration of CS was between 1.5 and 2 wt %.

Validation of the combined RSM model of size and stability for CS-Se NPs

Figure 4 shows the combined contour plot of zeta potential and size with Na_2SeO_3 and ascorbic acid as X and Y axis, keeping the concentration of CS at a constant value.

From the RSM model of CS-Se NP, it was evident that concentration of Na_2SeO_3 and ascorbic acid have a significant effect on the variation of its size and stability while CS has not shown any influence. The white

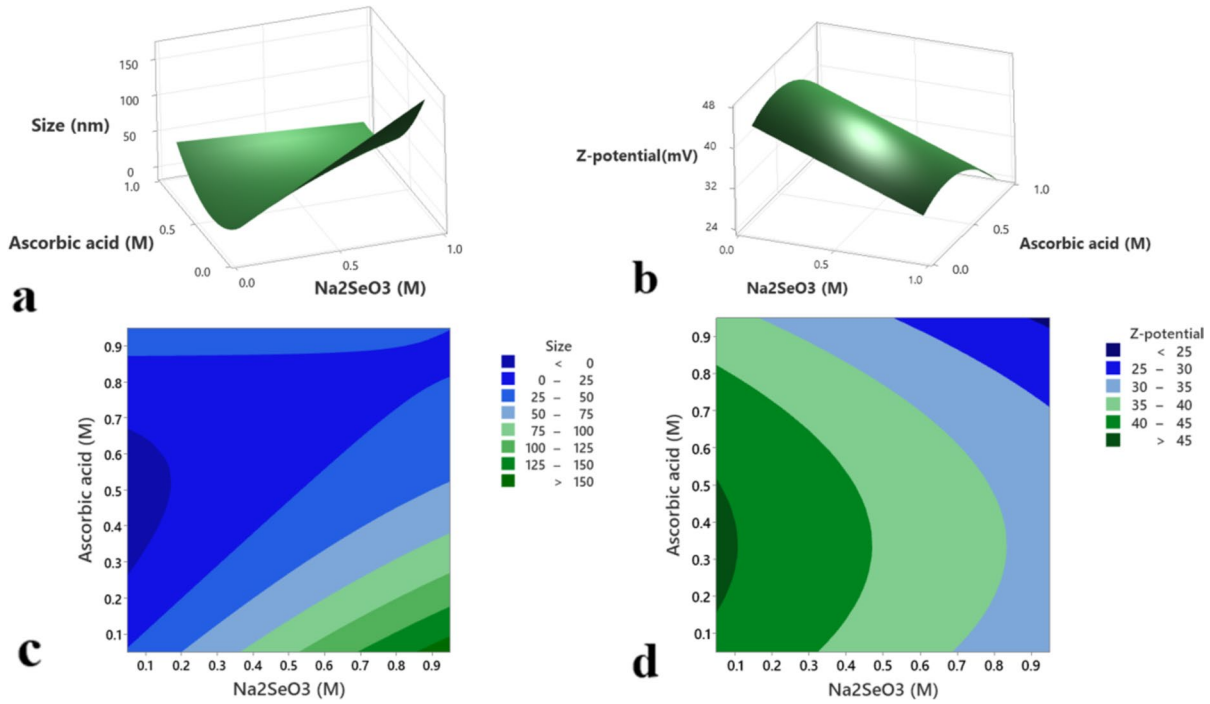

Fig. 3 For CS-NPs: **a** surface plot of size; **b** surface plot of zeta potential; **c** two-dimensional contour plot for size; **d** two-dimensional contour plot for zeta potential

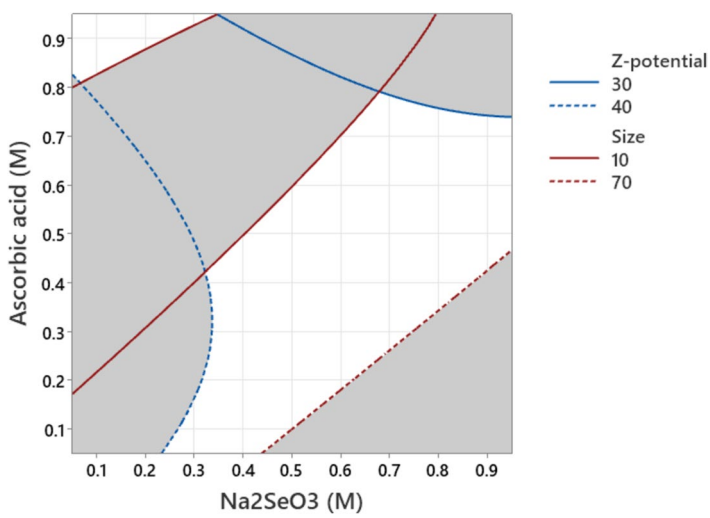

Fig. 4 Combined contour plot of zeta potential and size for CS-Se NPs

colored region in the combined contour plot of size and stability of CS-Se NPs is the area of interest and is used for the validation of the model. To do this, nanoparticles of size and stability in between 10 and 70 nm and 30–40 mV were synthesized. The size and stability of the NPs will be in this range when the concentration of Na_2SeO_3 and ascorbic acid were 0.7 M while the concentration of CS was 1.8 wt %. The Se NPs were capped by the CS molecules giving the mentioned stability and size to the nanoparticles. The positive value of zeta potential is due to the fact that the nanoparticles were modified on the surface by the positively charged

Table 4 Determination of Se NP size and zeta potential at different CCNF concentrations

Run	Size (nm)		Zeta potential (mV)	
	Average	SD	Average	SD
16	70.2	0.8	28.0	1.2
17	59.8	15.3	45.7	0.5
18	69.0	3.6	29.6	1.4
19	33.6	0.4	20.1	0.8
20	34.5	1.6	25.8	0.9
21	152.5	1.7	37.8	0.9
22	72.0	1.0	17.6	1.8
23	363.5	17.9	25.3	0.1
24	70.7	0.2	22.2	0.7
25	65.5	23.5	28.5	0.9
26	82.9	0.4	27.0	0.1
27	84.4	1.3	33.4	0.8
28	124.8	1.7	28.0	0.4
29	272.3	8.6	32.9	1.8
30	81.8	1.4	26.3	1.4

CS molecules. This surface interactions resulted in the improved stability and smaller size for Se NPs.

RSM model for optimization of size and zeta potential of CCNF-Se NPs

The results of Table 4 indicate that CCNFs can significantly influence the size and stability of Se NPs. Optimal concentrations seem to produce nanoparticles in the 60–90 nm range with zeta potential values indicating good stability. However, some conditions lead to much larger sizes, likely due to aggregation. The high variability in some measurements suggests that fine-tuning the concentration of CCNFs is crucial for obtaining consistent and stable nanoparticles.

Statistical analysis was conducted using CCD model for CCNF-Se NPs similar to that of CS-Se NPs. Different concentration of Na_2SeO_3, CCNFs, and ascorbic acid was used as the three independent variables and the responses were size and zeta potential. 15 sets of experiments were conducted using different concentrations of the variables and their responses were noted and the model was plotted. A, B, C corresponds to concentration of Na_2SeO_3, CCNFs, and ascorbic acid respectively. It was clear from the Pareto chart (Fig. 5a and b) of CCNF-Se NPs that A and C contribute significantly to the variation in size while almost all variables have a significant effect on the zeta potential. In the case of size of CCNF-Se NPs, interaction between A and C were significant whereas there were significant interactions between A, B, and C for the zeta potential.

The model F-value for size and zeta potential was 5.76 and 34.32 respectively. Since the value exceeds 1, it indicates that the model was significant. Additionally, the model p-value was found to be 0.013 and 0.00 for size and zeta potential, respectively. This small value proves again the statistical significance of the model. The p-value for A and C in the analysis of variance of size and A, B, C in the analysis of variance of zeta potential is less than 0.05 indicating that they contribute significantly to the data variability. The F value is higher for A (Na_2SeO_3) and C (ascorbic acid) for size

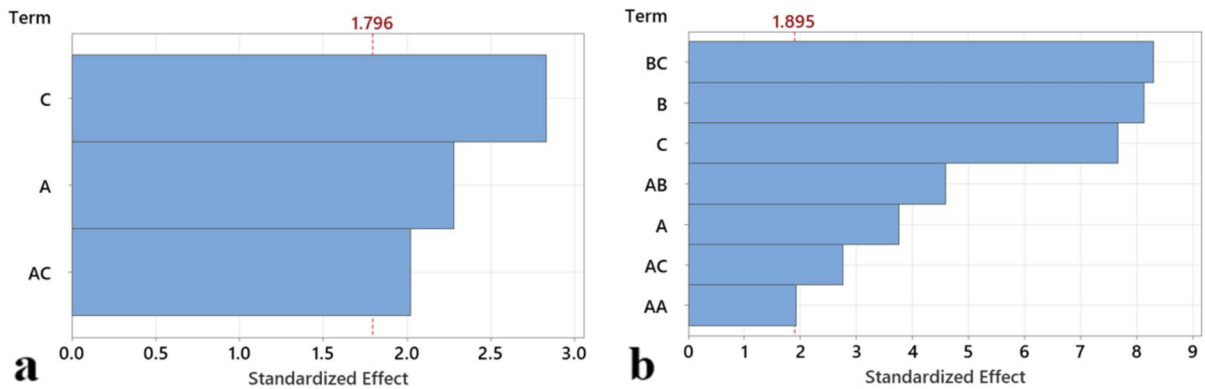

Fig. 5 Pareto chart of **a** size and **b** zeta potential of CCNF-Se NPs

Table 5 Analysis of variance of size and zeta potential of CCNF-Se NPs

Analysis of Variance (significant values)	Size		Zeta potential	
	F-Value	P-Value	F-Value	p-Value
Model	5.76	0.013	34.32	0.000
Linear	6.60	0.013	46.29	0.000
Na2SeO3	5.19	0.044	14.14	0.007
CCNF	Neglected		66.03	0.000
Ascorbic acid	8.01	0.016	58.69	0.000
Na2SeO3*Na2SeO3	Neglected		3.72	0.095
Na2SeO3*CCNF			21.12	0.002
Na2SeO3*Ascorbic acid	4.07	0.069	7.57	0.028
CCNF*Ascorbic acid	Neglected		68.94	0.000

while it is higher for A (Na_2SeO_3), B (CCNFs), and C (ascorbic acid) for zeta potential in the analysis of variance that is shown in Table 5. The F values were in accordance with the Pareto chart since the latter also exhibits the same trend. All the variables have a significant contribution in varying the zeta potential of the CCNF-Se NPs while only two for the size. The R^2 value from the model summary for the size and zeta potential of CCNF-Se NPs was found to be 0.61 and 0.97 respectively. So, from the F, P and R^2 value, it can be concluded that the model thus designed was statistically significant. Upon regression analysis we could obtain Eq. 6 and 7 for size and zeta potential and the variables were then expressed using their coded values, where A, B, C represents Na_2SeO_3, CCNFs, and ascorbic acid respectively.

$$\text{Size} = 66.5 + 215.0A - 14.5C - 225.2A * C \quad (6)$$

$$\begin{aligned}\text{Zeta potential} &= 46.24 + 1.63A - 26.68B \\ &\quad - 16.91C - 8.662A * A + 12.61A * B \\ &\quad - 7.97A * C + 22.79B * C\end{aligned} \quad (7)$$

To determine the optimum concentration required for the synthesis of small and highly stable NPs, surface response graphs, main effect, and contour graphs were plotted using the software.

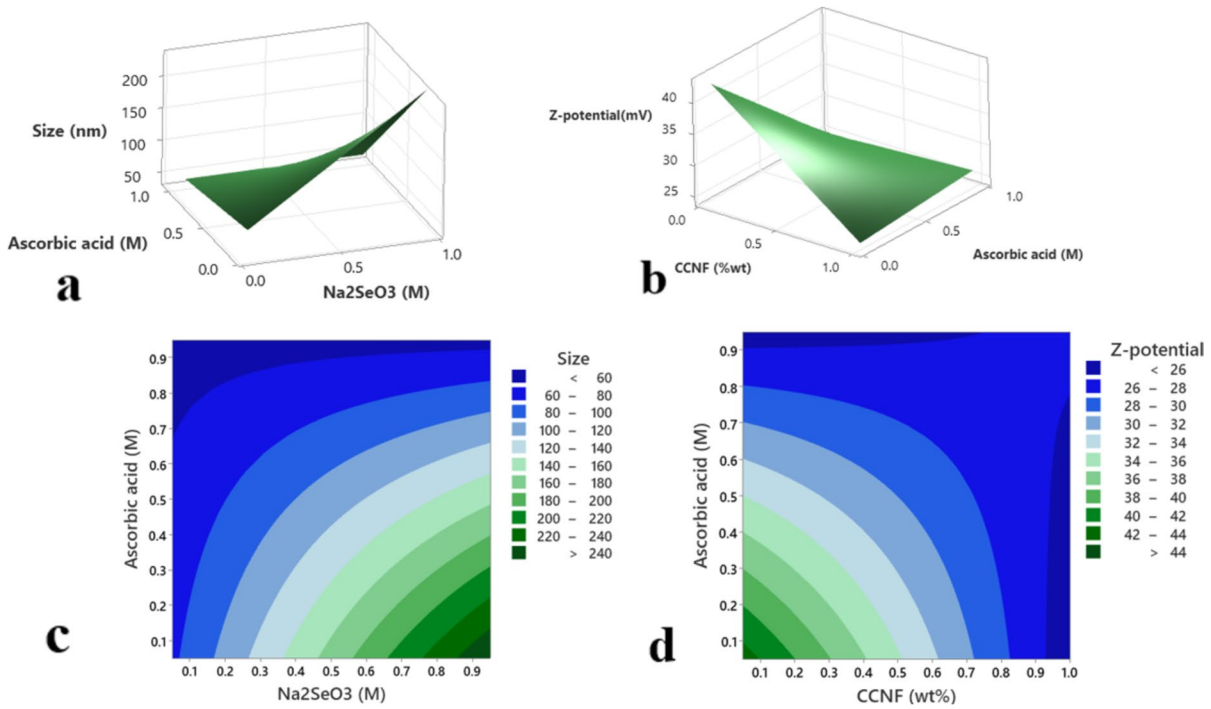

Fig. 6 Three-dimensional Surface plots of **a** size **b** zeta potential for CCNF-Se NPs. Two-dimensional contour plot for **c** size, **d** zeta potential of CCNF-Se NPs

Figure 6a and b shows the three-dimensional surface plot of size and zeta potential of CCNF-Se NPs. Surface plots demonstrate the mutual interaction between two targeted variables on the size and stability of the CCNF-Se NPs by converting the data into a three-dimensional diagram. The two-dimensional (2D) contour plot (Fig. 6c and d), generated from the pairwise combination of variables while holding other variables at their center point level, demonstrates the mutual interaction of the independent factors. The fixed variables in all the surface and contour graphs were held constant at values 0.5 M for both Na_2SeO_3 and ascorbic acid while it was 0.525% wt for CCNFs. From these graphs along with the two-dimensional contour plot, it can be partly assured that highly stable and small sized nanoparticles can be obtained if we use concentrations of ascorbic acid to be 0.5 M and that of Na_2SeO_3 and CCNFs to be in the range between 0.05 and 0.5 M and 0.05–0.5% wt respectively. The same results can be derived from the main effect plot of size and zeta potential of CCNF-Se NPs (Fig. 3 Sa and Sb).

Contour plot of zeta potential and size

The combined contour graph (Fig. 7) of zeta potential and size of CCNF-Se NPs were plotted using the values of size and zeta potential that we obtained by using different combinations of variables as the 15 sets of experiments that we designed, and it was validated. From this validation it was observed that the stable Se NPs of size and zeta potential in between 50 and 85 nm and 30–35 mV could be synthesized when the concentration of Na_2SeO_3 and ascorbic acid were 0.3 M and 0.5 M respectively. 0.3% wt of CCNFs was added to the above mixture which acts as a stabilizing agent to stabilize the Se NPs formed.

CS-Se NPs and CCNF-Se NPS were prepared based on the concentrations obtained from the validated model. From the synthesis of Se NPs using two different stabilizers, it was found that the size of CCNF-Se NPs was a little bit larger than the CS-Se NPs. It was proved that we can obtain CS-Se NPs of size and zeta potential in the range 10–70 nm and 30–40 mV, respectively, when the concentration of Na_2SeO_3 and ascorbic acid were 0.7 M and CS was 1.8 wt %. In the case of CCNF-Se NP, it was found that we could obtain size and zeta potential between 50 and 85 nm and 30–35 mV, respectively, when the concentrations of Na_2SeO_3, ascorbic acid, and CCNFs were 0.3 M, 0.5 M, and 0.3% wt respectively.

Synthesis of optimized Se NPs

Experimental validation of optimized parameters was carried on. In the case of Se NPs using CS as a stabilizer, 100 mL of 0.7 M ascorbic acid, 1 mL of 1.8 wt % CS solution were used. Contrary, for the Se NPs using CCNFs as a stabilizing agent, 100 mL of 0.5 M ascorbic acid, 0.3 g of CCNFs, and 1 mL of 0.3 M Na_2SeO_3 were used. Their formation was confirmed by the SPR band in the UV–Vis spectra which

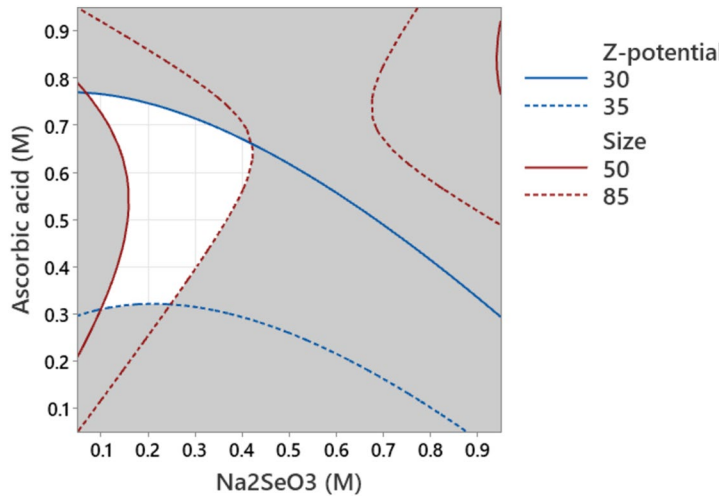

Fig. 7 Combined contour plot of zeta potential and size of CCNF-Se NPs

was done after their synthesis. DLS of the above prepared CS-Se NP and CCNF-Se NP solution was done to determine its size and zeta potential. The colour of the solution will change from colourless to dark orange-red upon the addition of the precursor which indicates the formation of nanoparticles.

UV–Vis spectrophotometry

The initial confirmation of CS-Se NPs and CCNF-Se NP formation was achieved through plasmon resonance using UV–Visible spectrophotometry. The color change from colorless to bright orange red was an indication for the reduction Na_2SeO_3 to elemental Se, that is, Se (0) and was due to the excitation of surface plasmon resonance (SPR). The UV–Vis spectrum of the synthesized CS-Se NPs and CCNF-Se NPs were given in Fig. 8. Also, an inset image of the Se NPs synthesized using CS and CCNFs is provided in the UV–Vis spectra.

For CS-Se NPs, the SPR band was obtained at 253.31 nm while it was at 255.22 nm for CCNF-Se NPs. The band in this range confirms the formation of Se NPs, consistent with previous studies. Lunko et al. (Lunkov et al. 2023) synthesized Se NP stabilized by quaternized chitosan derivatives and observed SPR band at 262–293 nm. A SPR band at 217 and 278 nm was observed by Elsayed et al. for the synthesized Se NPs (Elsayed, Hasanin, and Abdelraof 2022). Gunti et al. (Gunti et al. 2019) prepared Se NPs from *Embilica officinalis* fruit extract and observed SPR band at 270 nm. Similarly, an UV–Vis absorption maximum at 261 nm was obtained through the green synthesized Se NPs from *Diospyros montana* leaf extract (Kokila et al. 2017). It was found that when the size of the Se NPs is above 100 nm it will show a band above 300 nm (Shah et al. 2010). So, the peak that was obtained in this study proves the formation of nanoparticles of smaller size. Se NPs synthesized using two different stabilizers (CS, CCNFs) exhibit almost similar color and characteristic SPR band.

Dynamic light scattering measurements (DLS)

The size and zeta potential of the synthesized and RSM-optimized nanoparticles were determined using DLS measurements. Zeta potential was a crucial property for evaluating the current state of nanoparticles and their stability in solution (Molina et al. 2011). DLS measurements confirmed that Se NPs synthesized using CS as a stabilizer have size ranging from 10 to 70 nm and zeta potential between 30 and 40 mV (Fig. 3S a and b). In comparison, Se NP stabilized with CCNFs exhibit size between 50 and 85 nm and zeta potential of 30–35 mV (Fig. 4S c and d). The positive zeta potential is attributed to the presence of positively charged CS and CCNFs on the surface of the Se NPs. These positively charged molecules cap the nanoparticles, inducing

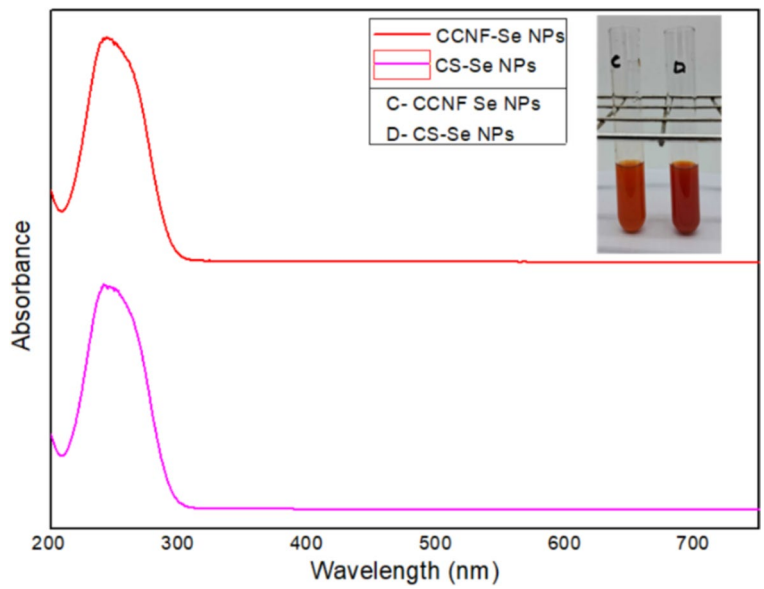

Fig. 8 Normalized and shifted UV–Vis spectra of Cs-Se NPs and CCNF-Se NPs

stability and preventing aggregation. Higher zeta potential values correlate with increased nanoparticle stability due to greater electrostatic repulsion between nanoparticles. CS and CCNFs surface modified Se NPs remain stable and monodispersed in the medium due to the positive charge imparted by the stabilizing agents. This positive charge generates repulsive forces, which prevent nanoparticle aggregation. Narrow peaks in the DLS spectra of CS-Se NPs and CCNF-Se NPs indicate that the nanoparticles are monodispersed, also they have polydispersity index of 0.21 for CS-Se NPs and 0.16 for CCNF-Se NPs, which suggests minimum particle aggregation. The primary focus of this work was the synthesis of stable, small-sized nanoparticles, which was successfully achieved in this experiment. It was found that the size and zeta potential of both CS stabilized and CCNFs stabilized nanoparticles were very much alike. Thus, the production of nanosized, stable nanoparticles has been confirmed by DLS measurements.

FESEM

FESEM analysis confirmed the morphology of the synthesized Se NPs. These images reveal that CS-Se NPs and CCNF-Se NPs were spherical in shape. Figure 9a show the FESEM images of Se NP stabilized by CS while Fig. 9b shows Se NP stabilized by CCNF with marked sizes of NPs. The Se NPs were uniformly dispersed in the medium without any aggregation. CCNFs demonstrates similar stabilizing properties to CS, ensuring uniform dispersion in the medium. This confirms that both CS-Se NPs and CCNF-Se NPs are almost identical, spherical, and highly stable, as indicated by their high zeta potential.

CS and CCNFs serve as both stabilizing and capping agents, significantly affecting the size and stability of synthesized Se NPs under consistent conditions. Their capping action results in a uniform distribution of nanoparticles due to the positively charged CS and CCNF molecules, which impart a positive charge to the nanoparticles. This positive charge induces repulsive forces, preventing aggregation and promoting uniform distribution. The size and shape of the nanoparticles synthesized using both stabilizers were very much alike and spherical. Additionally, the synthesized nanoparticles fall within the range specified in the RSM model, validating the model's accuracy and error-free performance based on the size and stability of the nanoparticles. The results obtained from FESEM images were consistent with the DLS analysis, although the sizes of the Se NPs were slightly larger in the DLS measurements. This discrepancy could be attributed to the hydrodynamic coating of water molecules around the CS-Se NPs and CCNF-Se NPs in the case of DLS measurements.

Moreover, the synthesized Se NP stabilized by CS and CCNFs showed greater stability and smaller size compared to the nanoparticles synthesized

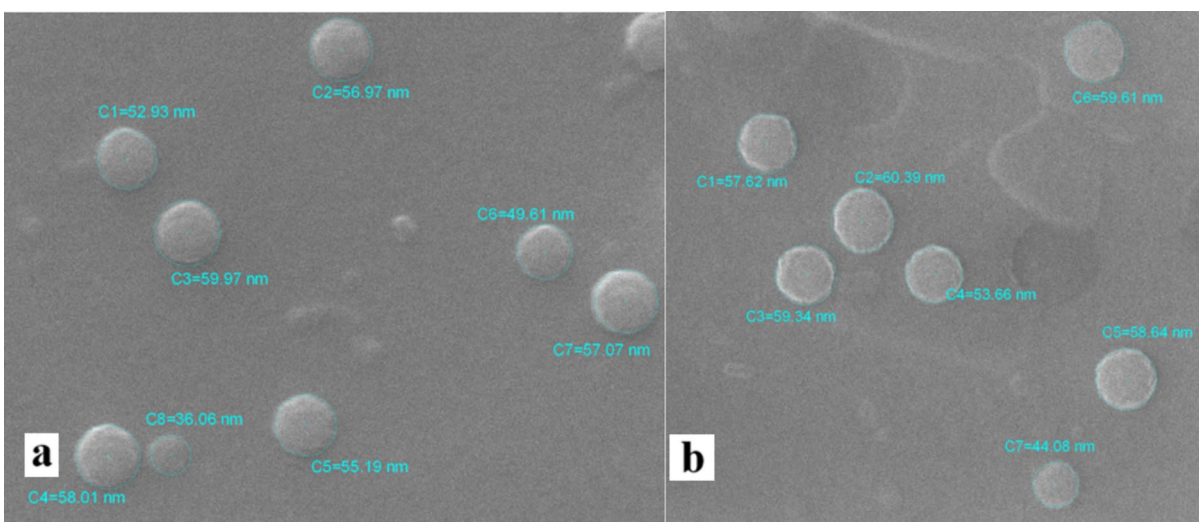

Fig. 9 FESEM image of **a** CS-Se NPs and **b** CCNF-Se NPs. Numbers indicate particle diameter

through non-green methods. Xia et al. (Xia et al. 2018) synthesized Se NPs decorated with the polycationic polymers like polyethyleneimine (PEI) linked with folic acid (FA). The size of the modified NPs were ~ 115 nm and a zeta potential of 19.4 mV. Gangadoo et al. (Gangadoo et al. 2017) used poly sodium 4-styrenesulfonate (PSSS) as a stabilizer to synthesize Se NPs of size 46 nm and zeta potential of 0.8 mV. Polyvinyl alcohol (PVA) stabilized Se NPs of size 20–80 nm was synthesized by Shah et.al (Shah et al. 2007). Se NPs synthesized using CS and CCNFs as stabilizer represent a sustainable and green method, as we could obtain Se NPs with smaller, comparable size, and improved stability when compared with the former studies mentioned above. The stabilizing agents used in the former studies are not sustainable materials when compared with the stabilizers used in this work. The key aspect is that we could prepare Se NPs of comparable size and improved zeta potential value compared to those synthesized using non-eco-friendly method. The method we used was low cost, efficient and green.

Energy dispersive X-ray spectroscopy (EDX)

EDX spectra were measured in conjunction with FESEM. The strong peaks in the EDX spectra confirmed that the spherical nanoparticles are selenium. Figure 10 depicts the EDX spectra of CS-Se NPs and CCNF-Se NPs, showing a distinct peak for Se. This confirms the formation of elemental Se NPs which being spherical in shape. The synthesized Se NPs showed characteristic absorption peaks of Se at 1.37 keV and 11.22 keV (Sharma et al. 2014). Carbon (C) and oxygen (O) peak in the spectra confirms the presence of stabilizers which were composed of alkyl chains. So, these peaks confirm the formation of elemental selenium and their interaction with CS and CCNFs.

X-ray diffraction analysis (XRD)

The XRD patterns of CS-Se NPs and CCNF-Se NPs are displayed in Fig. 11. Sharp Bragg peaks indicate the presence of selenium crystallites. Out of the different allotropes that elemental selenium may adopt, α-monoclinic Se is generally favored for nanoparticle synthesis from a selenium(IV) precursor (Lin and Wang 2005). In any case, the occurrence of conductive hexagonal Se crystals is neglected in light of the color of the Se NPs presented here (orange to deep red, not metallic grey) (Ruiz-Fresneda et al. 2023), the failure to observe hexagonal rods by electronic microscopy, and the XRD patterns themselves.

α-Se has been reported to have lattice constants of values a = 11.60 Å, b = 9.08 Å, and c = 14.82 Å (Cherin and Unger 1972). Crystallographic planes (020), (101), (200), (31–2), (30–1), and (122) were assigned to the diffraction peaks of 2θ = 19.9°, 20.9°, 25.2°, 27.8°, 29.8°, and 35.5°, respectively. That said, given the multiplicity of diffraction peaks, the presence of other monoclinic or amorphous phases should not be disregarded.

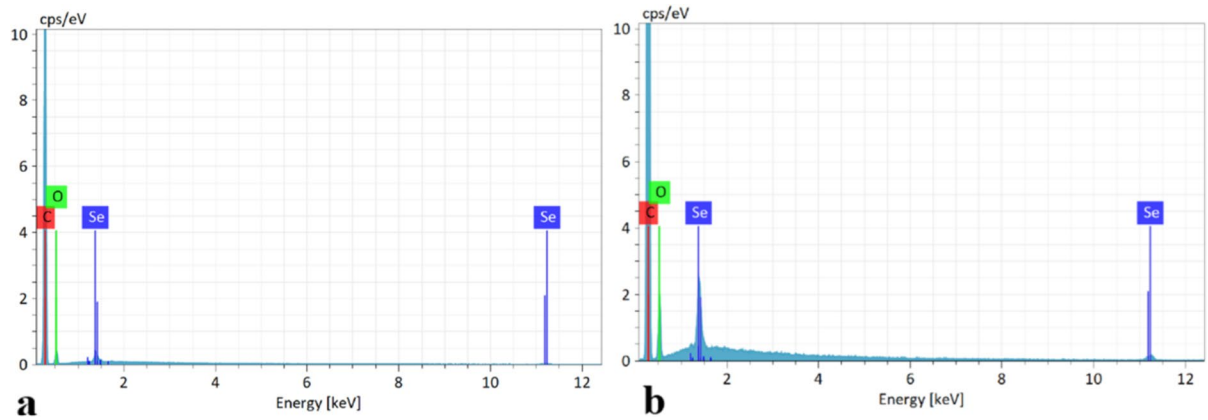

Fig. 10 EDX spectra of **a** CS-Se NPs, **b** CCNF-Se NPs

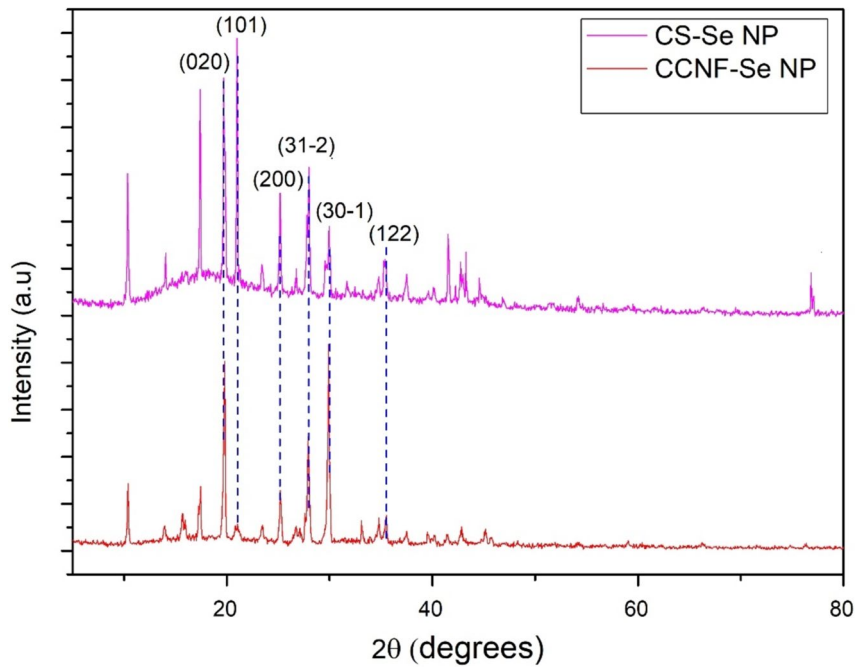

Fig. 11 XRD patterns of synthesized CS-Se NP and CCNF-Se NP

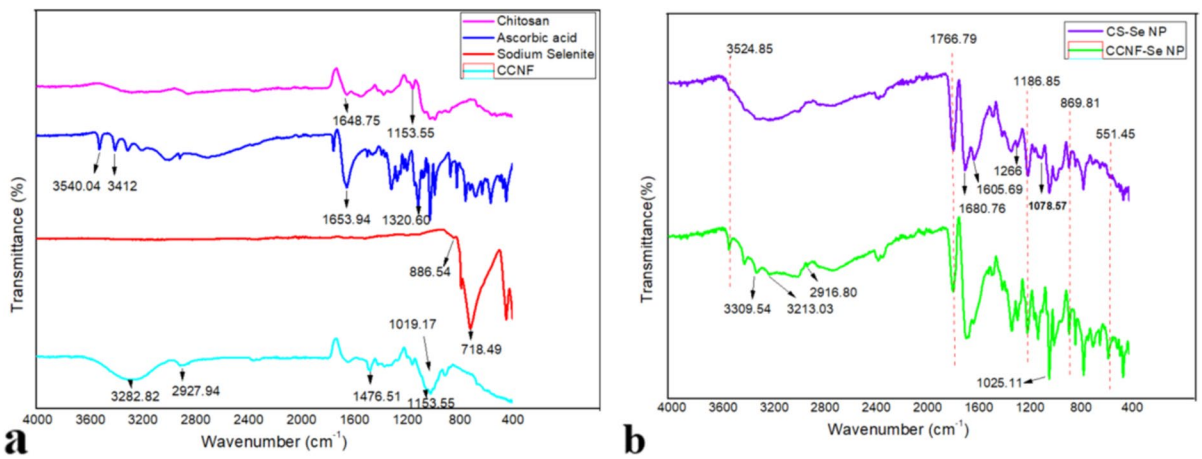

Fig. 12 **a** FT-IR spectra of all the reagents used; **b** combined FT-IR spectra of CS-Se NP and CCNF-Se NP

Fourier transform infrared spectroscopy (FT-IR)

FTIR analysis was used to find the functional groups by measuring the vibrational frequencies of chemical bonds present on the surface of the synthesized Se NPs. The intense peak at 3540.04 cm^{-1} of ascorbic acid (Fig. 12 a) was shifted to 3524.85 cm^{-1} of CS-Se NPs (Fig. 12b), which indicate that the Se has interacted with the hydroxyl group of ascorbic through hydrogen bonding and facilitated in the Se NP synthesis. Peaks at 1653.94 cm^{-1} and 1320.60 cm^{-1} correspond to the stretching vibration of C–C double bond and the peak of enol-hydroxyl respectively of L-ascorbic acid. The bands at 714 and 551.45 cm^{-1} indicate the binding of Se NPs with hydroxyl groups, forming Se-O bonds. This suggests the presence of coordination bonds between selenium and ascorbic acid. 869.81 cm^{-1} and 1266 cm^{-1} peaks in the CS-Se NPs correspond to the saccharide structure of chitosan and it indicate the presence of chitosan on the

surface of the Se NPs. Thus, it can be proved that Se NPs were surface functionalized by the CS molecules.

The peak at 3282.82 cm^{-1} is due to the O–H group of CCNF and it was shifted to 3213.03 cm^{-1} in CCNF-Se NPs which suggest that the Se has interacted with hydroxyl groups in cationic cellulose nanofibers and has been surface functionalized. The peak at 1153.55 cm^{-1} is due to the C–C ring stretching band in the CCNFs. The peak at 2927.94 cm^{-1} is due to C-H moieties of cellulose in the CCNFs and was shifted to 2916.80 indicating that Se interacted with CCNFs and has been surface functionalized. These results confirm the role of the reducing and stabilizing (CS & CCNFs) agents in the synthesis of Se NPs.

Conclusions

In the present study, Se NPs were successfully synthesized using a green chemical reduction method employing CCNFs for the first time or CS as stabilizing agents while Na_2SeO_3 as the metal precursor and L-ascorbic acid as the reducing agent. The Se NPs aggregation was eliminated by the presence of the stabilizing agents like CCNFs or CS. The positively charged CCNFs or CS act as a capping agent for the negatively charged Se NPs providing a steric hindrance and electrostatic repulsion which prevented their particle aggregation. The anionic demand of CCNFs was 2000 μeq/g and nano fibrillation yield was found to be greater than 95%. An experimental design was used to optimize nanoparticles size and stability, focusing on reagent concentrations as three independent variables. The RSM model for CS and CCNFs stabilized nanoparticles was validated using the CCD approach. The R^2 value obtained for size and stability for both CS-Se NPs and CCNF-Se NPs were close to 1 indicating that the variables really fitted into the model and the model was error-free and significant. The model was optimized and CS-Se NPs of size and zeta potential in between 10 and 70 nm and 30–40 mV was synthesized when the concentration of Na_2SeO_3 and ascorbic acid were 0.7 M and 1.8%wt. of CS. While CCNF-Se NPs of size and zeta potential value between 50 and 85 nm and 30–35 mV were synthesized when the concentration of the precursor, reducing agent, and CCNFs (stabilizer) were 0.3 M, 0.5 M, and 0.3%wt. The uniform distribution and spherical shape of the synthesized CS-Se NPs and CCNF-Se NPs was proved by FESEM, and their size was measured by DLS. The interaction between the stabilizing agent and Se NPs was confirmed using the FTIR technique. The formation of elemental Se and their crystalline nature was established by the EDS and XRD spectra. Thus, in this work, small and stable CS-Se NPs and CCNF-Se NPs were efficaciously synthesized and optimized using RSM-CCD modeling.

Acknowledgments Authors wish to acknowledge the financial support of the funding agencies listed in the Funding section. Marc Delgado-Aguilar and Quim Tarrés are Serra Húnter Fellows. Samanta Sam is grateful for the support of the predoctoral program AGAUR-FI grants (2023 FI-3 00065) Joan Oró from the Secretariat of Universities and Research of the Department of Research and Universities of the Generalitat de Catalunya and the European Social Fund Plus.

Author's contributions S.S: Experimental, Data curation, Writing—Original Draft; N.F: Conceptualization, Supervision, Writing—Original Draft; R.J.A.: Methodology, Writing—Review and Editing; E.S.: Methodology, Writing—Review and Editing; F.C.: Writing—Review and Editing; M.D-A.: Conceptualization, Writing—Review and Editing, Project administration, Funding acquisition; Q.T.: Conceptualization, Supervision, Writing—Review and Editing, Project administration, Funding acquisition;

Funding Open Access funding provided thanks to the CRUE-CSIC agreement with Springer Nature. This research was received from the Spanish Ministry of Science and Innovation, project NextPack (PID2021-124766OA-I00).

Data availability No datasets were generated or analysed during the current study.

Declarations

Conflict of interest The authors declare no competing interests.

Ethical approval The authors declare that this manuscript is not under consideration by any other journal at the time of submission. The submitted work is original, has not been published elsewhere in any form, and is not part of a larger study. All results are presented with integrity, adhering to principles of honesty without fabrication, falsification, or inappropriate data manipulation. Additionally, no data, text, or theories from others are misrepresented as our own.

Consent for publication All authors have reviewed the final version of the manuscript and approve its submission.

References

Abdelhamid AE, Ahmed EH, Awad HM, Ayoub MMH (2024) Synthesis and cytotoxic activities of selenium nanoparticles incorporated nano-chitosan. Polym Bull 81:1421–1437. https://doi.org/10.1007/s00289-023-04768-8

Ahmadi A, Ahmadi P, Sani MA et al (2021) Functional biocompatible nanocomposite films consisting of selenium and zinc oxide nanoparticles embedded in gelatin/cellulose nanofiber matrices. Int J Biol Macromol 175:87–97. https://doi.org/10.1016/j.ijbiomac.2021.01.135

Akram W, Mia R, Ullah S et al (2024) Simultaneous synthesis and application of TiO_2 nanoparticles using mulberry leaves for functionalization of organic cotton fabric. J Clean Prod. https://doi.org/10.1016/j.jclepro.2024.140939

Al Jahdaly BA, Al-Radadi NS, Eldin GMG et al (2021) Selenium nanoparticles synthesized using an eco-friendly method: dye decolorization from aqueous solutions, cell viability, antioxidant, and antibacterial effectiveness. J Mater Res Technol 11:85–97. https://doi.org/10.1016/j.jmrt.2020.12.098

Amado IR, Franco D, Sánchez M et al (2014) Optimisation of antioxidant extraction from solanum tuberosum potato peel waste by surface response methodology. Food Chem 165:290–299. https://doi.org/10.1016/j.foodchem.2014.05.103

Bisht N, Phalswal P, Khanna PK (2022) Selenium nanoparticles: a review on synthesis and biomedical applications. Mater Adv 3:1415–1431. https://doi.org/10.1039/d1ma00639h

Chen Y, Stoll S, Sun H et al (2022) Stability and surface properties of selenium nanoparticles coated with chitosan and sodium carboxymethyl cellulose. Carbohydr Polym 278:118859. https://doi.org/10.1016/j.carbpol.2021.118859

Cherin P, Unger P (1972) Refinement of the crystal structure of α-monoclinic Se. Acta Crystallogr Sect B Struct Crystallogr Cryst Chem 28:313–317. https://doi.org/10.1107/S0567740872002249

Dong BH, Hinestroza JP (2009) Metal nanoparticles on natural cellulose fibers: Electrostatic assembly and in situ synthesis. ACS Appl Mater Interfaces 1:797–803. https://doi.org/10.1021/am800225j

Fatma A, El L, Gharib IM et al (2019) The response of cowpea (Vigna unguiculata L) plants to foliar application of sodium selenate and selenium nanoparticles (SeNPs). J Nanomater Mol Nanotechnol 8:4. https://doi.org/10.4172/2324-8777.1000272

Gangadoo S, Stanley D, Hughes RJ et al (2017) The synthesis and characterisation of highly stable and reproducible selenium nanoparticles. Inorg Nano-Met Chem 47:1568–1576. https://doi.org/10.1080/24701556.2017.1357611

Ghelich R, Jahannama MR, Abdizadeh H et al (2019) Central composite design (CCD)-response surface methodology (RSM) of effective electrospinning parameters on PVP-B-Hf hybrid nanofibrous composites for synthesis of HfB 2 -based composite nanofibers. Compos B Eng 166:527–541. https://doi.org/10.1016/j.compositesb.2019.01.094

Gunti L, Dass RS, Kalagatur NK (2019) Phytofabrication of selenium nanoparticles from emblica officinalis fruit extract and exploring its biopotential applications: antioxidant, antimicrobial, and biocompatibility. Front Microbiol 10:1–17. https://doi.org/10.3389/fmicb.2019.00931

Hasanin MS, Hashem AH, Al-Askar AA, Haponiuk J, Saied E (2023) A novel nanocomposite based on mycosynthesized bimetallic zinc-copperoxide nanoparticles, nanocellulose and chitosan: characterization, antimicrobial and photocatalytic activities. Electron J Biotechnol 65:45–55. https://doi.org/10.1016/j.ejbt.2023.05.001

Harper BJ, Clendaniel A, Sinche F et al (2016) Impacts of chemical modification on the toxicity of diverse nanocellulose materials to developing zebrafish. Cellulose 23:1763–1775. https://doi.org/10.1007/s10570-016-0947-5

Hosnedlova B, Kepinska M, Skalickova S et al (2018) Nano-selenium and its nanomedicine applications: a critical review. Int J Nanomedicine 13:2107–2128. https://doi.org/10.2147/IJN.S157541

Hu T, Li H, Zhao G, Guo Y (2021) Selenium enriched hypsizygus marmoreus, a potential food supplement with improved Se bioavailability. Lwt 140:110819. https://doi.org/10.1016/j.lwt.2020.110819

Islam MS, Chen L, Sisler J, Tam KC (2018) Cellulose nanocrystal (CNC)-inorganic hybrid systems: synthesis, properties and applications. J Mater Chem B 6:864–883. https://doi.org/10.1039/c7tb03016a

Jang KH, Kang YO, Park WH (2014) Functional cellulose-based nanofibers with catalytic activity: efect of Ag content and Ag phase. Int J Biol Macromol 67:394–400. https://doi.org/10.1016/j.ijbiomac.2014.03.052

Kapur M, Soni K, Kohli K (2017) green synthesis of selenium nanoparticles from Broccoli, characterization, application and toxicity. Adv Tech Biol Med 05:1–7. https://doi.org/10.4172/2379-1764.1000198

Khan I, Saeed K, Khan I (2019) Nanoparticles: properties, applications and toxicities. Arab J Chem 12:908–931. https://doi.org/10.1016/j.arabjc.2017.05.011

Kokila K, Elavarasan N, Sujatha V (2017) Diospyros montana leaf extract-mediated synthesis of selenium nanoparticles and their biological applications. New J Chem 41:7481–7490. https://doi.org/10.1039/c7nj01124e

Kumar JA, Krithiga T, Manigandan S et al (2021) A focus to green synthesis of metal/metal based oxide nanoparticles: various mechanisms and applications towards ecological approach. J Clean Prod 324:129198

Lalegani Z, Seyyed Ebrahimi SA (2020) Optimization of synthesis for shape and size controlled silver nanoparticles using response surface methodology. Colloids Surf A

Physicochem Eng Asp 595:124647. https://doi.org/10.1016/j.colsurfa.2020.124647
Lin Z-H, Wang CR (2005) Evidence on the size-dependent absorption spectral evolution of selenium nanoparticles. Mater Chem Phys 92:591–594. https://doi.org/10.1016/j.matchemphys.2005.02.023
Liu Y, Kang S, Li K et al (2022) Ecofriendly and enhanced biogenic synthesis of silver nanoparticles using deep eutectic solvent-based green tea extracts. J Clean Prod. https://doi.org/10.1016/j.jclepro.2022.134655
Long K, Liu J, Zhang S et al (2024) Production of highly substituted cationic cellulose nanofibrils through disk milling/high-pressure homogenization. Cellulose 31:4217–4230. https://doi.org/10.1007/s10570-024-05861-5
Luesakul U, Komenek S, Puthong S, Muangsin N (2016) Shape-controlled synthesis of cubic-like selenium nanoparticles via the self-assembly method. Carbohydr Polym 153:435–444. https://doi.org/10.1016/j.carbpol.2016.08.004
Lunkov A, Konovalova M, Shagdarova B et al (2023) Synthesis of selenium nanoparticles modified by quaternary chitosan covalently bonded with gallic acid. Polymers (Basel) 15:1–12. https://doi.org/10.3390/polym15092123
Luo Y, Ren Z, Bo R et al (2020) Designing selenium polysaccharides-based nanoparticles to improve immune activity of Hericium erinaceus. Int J Biol Macromol 143:393–400. https://doi.org/10.1016/j.ijbiomac.2019.12.061
Modrzejewska-Sikorska A, Konował E, Klapiszewski Ł et al (2017) Lignosulfonate-stabilized selenium nanoparticles and their deposition on spherical silica. Int J Biol Macromol 103:403–408. https://doi.org/10.1016/j.ijbiomac.2017.05.083
Molina R, Al-Salama Y, Jurkschat K et al (2011) Potential environmental influence of amino acids on the behavior of ZnO nanoparticles. Chemosphere 83:545–551. https://doi.org/10.1016/j.chemosphere.2010.12.020
Ndwandwe BK, Malinga SP, Kayitesi E, Dlamini BC (2021) Advances in green synthesis of selenium nanoparticles and their application in food packaging. Int J Food Sci Technol 56:2640–2650. https://doi.org/10.1111/ijfs.14916
Negm NA, Hefni HHH, Abd-Elaal AAA et al (2020) Advancement on modification of chitosan biopolymer and its potential applications. Int J Biol Macromol 152:681–702. https://doi.org/10.1016/j.ijbiomac.2020.02.196
Panahi-Kalamuei M, Salavati-Niasari M, Hosseinpour-Mashkani SM (2014) Facile microwave synthesis, characterization, and solar cell application of selenium nanoparticles. J Alloys Compd 617:627–632. https://doi.org/10.1016/j.jallcom.2014.07.174
Pedrosa JFS, Rasteiro MG, Neto CP, Ferreira PJT (2022) Effect of cationization pretreatment on the properties of cationic Eucalyptus micro/nanofibrillated cellulose. Int J Biol Macromol 201:468–479. https://doi.org/10.1016/j.ijbiomac.2022.01.068
Pei A, Butchosa N, Berglund LA, Zhou Q (2013) Surface quaternized cellulose nanofibrils with high water absorbency and adsorption capacity for anionic dyes. Soft Matter 9:2047–2055. https://doi.org/10.1039/c2sm27344f
Peng Y, Duan C, Elias R et al (2019) A new protocol for efficient and high yield preparation of cellulose nanofibrils. Cellulose 26:877–887. https://doi.org/10.1007/s10570-018-2112-9
Prasad R, Kumar V, Kumar M (2017) Nanotechnology: food and environmental paradigm. Nanotechnol Food Environ Paradig. https://doi.org/10.1007/978-981-10-4678-0
Pyrzynska K, Sentkowska A (2022) Biosynthesis of selenium nanoparticles using plant extracts. J Nanostructure Chem 12:467–480. https://doi.org/10.1007/s40097-021-00435-4
Ran M, Wu T, Jiao Y et al (2024) Selenium bio-nanocomposite based on extracellular polymeric substances (EPS): synthesis, characterization and application in alleviating cadmium toxicity in rice (Oryza sativa L.). Int J Biol Macromol. https://doi.org/10.1016/j.ijbiomac.2023.129089
Rasool A, Kiran S, Gulzar T et al (2023) Biogenic synthesis and characterization of ZnO nanoparticles for degradation of synthetic dyes: a sustainable environmental cleaner approach. J Clean Prod. https://doi.org/10.1016/j.jclepro.2023.136616
Rol F, Saini S, Meyer V et al (2019) Production of cationic nanofibrils of cellulose by twin-screw extrusion. Ind Crops Prod 137:81–88. https://doi.org/10.1016/j.indcrop.2019.04.031
Ruiz-Fresneda MA, Staicu LC, Lazuén-López G, Merroun ML (2023) Allotropy of selenium nanoparticles: colourful transition, synthesis, and biotechnological applications. Microb Biotechnol 16:877–892. https://doi.org/10.1111/1751-7915.14209
Sarwar N, Bin HU, Kumar M et al (2021) Citric acid mediated green synthesis of copper nanoparticles using cinnamon bark extract and its multifaceted applications. J Clean Prod. https://doi.org/10.1016/j.jclepro.2021.125974
Saylam E, Akkaya Y, Ilhan E et al (2021) Levodopa-loaded 3d-printed poly (Lactic) acid/chitosan neural tissue scaffold as a promising drug delivery system for the treatment of parkinson's disease. Appl Sci. https://doi.org/10.3390/app112210727
Serra-Parareda F, Aguado R, Tarrés Q et al (2021) Chemical-free production of lignocellulosic micro-and nanofibers from high-yield pulps: synergies, performance, and feasibility. J Clean Prod 313:127914
Shah CP, Dwivedi C, Singh KK et al (2010) Riley oxidation: a forgotten name reaction for synthesis of selenium nanoparticles. Mater Res Bull 45:1213–1217. https://doi.org/10.1016/j.materresbull.2010.05.013
Shah CP, Kumar M, Bajaj PN (2007) Acid-induced synthesis of polyvinyl alcohol-stabilized selenium nanoparticles. Nanotechnology. https://doi.org/10.1088/0957-4484/18/38/385607
Shakibaie M, Shahverdi AR, Faramarzi MA et al (2013) Acute and subacute toxicity of novel biogenic selenium nanoparticles in mice. Pharm Biol 51:58–63. https://doi.org/10.3109/13880209.2012.710241
Sharma G, Sharma AR, Bhavesh R et al (2014) Biomolecule-mediated synthesis of selenium nanoparticles using dried vitis vinifera (raisin) extract. Molecules 19:2761–2770. https://doi.org/10.3390/molecules19032761
Signori-Iamin G, Aguado RJ, Tarrés Q et al (2024) Exploring the synergistic effect of anionic and cationic fibrillated cellulose as sustainable additives in papermaking. Cellulose. https://doi.org/10.1007/s10570-024-06145-8

Skalickova S, Milosavljevic V, Cihalova K et al (2017) Selenium nanoparticles as a nutritional supplement. Nutrition 33:83–90. https://doi.org/10.1016/j.nut.2016.05.001

Sluiter A, Hames B, Ruiz R, et al (2008) Determination of Structural Carbohydrates and Lignin in Biomass. Laboratory Analytical Procedure (LAP) Issue Date: 7/17/2005

Štefanková D, Skrbek K, Pižl M, Bartůněk V (2023) Nano and mesosized selenium and its synthesis using the ascorbic acid route. J Non Cryst Solids. https://doi.org/10.1016/j.jnoncrysol.2023.122462

Tsimpliaraki A, Svinterikos S, Zuburtikudis I et al (2009) Nanofibrous structure of nonwoven mats of electrospun biodegradable polymer nanocomposites—A design of experiments (DoE) study. Ind Eng Chem Res 48:4365–4374. https://doi.org/10.1021/ie801327z

Vankudoth S, Dharavath S, Veera S et al (2022) Green synthesis, characterization, photoluminescence and biological studies of silver nanoparticles from the leaf extract of Muntingia calabura. Biochem Biophys Res Commun 630:143–150. https://doi.org/10.1016/j.bbrc.2022.09.054

Vijayaram S, Razafindralambo H, Sun YZ et al (2024) Applications of green synthesized metal nanoparticles—a review. Biol Trace Elem Res 202:360–386. https://doi.org/10.1007/s12011-023-03645-9

Wang G, Yang M, Li Z et al (2013) Synthesis and characterization of Zn-doped MgAl-layered double hydroxide nanoparticles as PVC heat stabilizer. J Nanopart Res. https://doi.org/10.1007/s11051-013-1882-0

Xia Y, Zhao M, Chen Y et al (2018) Folate-targeted selenium nanoparticles deliver therapeutic siRNA to improve hepatocellular carcinoma therapy. RSC Adv 8:25932–25940. https://doi.org/10.1039/c8ra04204g

Xiao X, Deng H, Lin X et al (2023) Selenium nanoparticles: properties, preparation methods, and therapeutic applications. Chem Biol Interact 378:110483. https://doi.org/10.1016/j.cbi.2023.110483

Xiong J, Wang Y, Xue Q, Wu X (2011) Synthesis of highly stable dispersions of nanosized copper particles using L-ascorbic acid. Green Chem 13(4):900–904. https://doi.org/10.1039/C0GC00772B

Ye X, Chen L, Liu L, Bai Y (2017) Electrochemical synthesis of selenium nanoparticles and formation of sea urchin-like selenium nanoparticles by electrostatic assembly. Mater Lett 196:381–384. https://doi.org/10.1016/j.matlet.2017.03.072

Yolmeh M, Jafari SM (2017) Applications of response surface methodology in the food industry processes. Food Bioproc Tech 10:413–433. https://doi.org/10.1007/s11947-016-1855-2

Zeng S, Ke Y, Liu Y et al (2018) Synthesis and antidiabetic properties of chitosan-stabilized selenium nanoparticles. Colloids Surf B Biointerfaces 170:115–121. https://doi.org/10.1016/j.colsurfb.2018.06.003

Zhai C, Lin Y, Mao C et al (2024) Construction, characterization, antioxidant activity and effects on properties in vitro digestion of selenium nanoparticles decorated with Cyperus esculentus polysaccharides. Food Biosci 59:104062. https://doi.org/10.1016/j.fbio.2024.104062

Zhang SY, Zhang J, Wang HY, Chen HY (2004) Synthesis of selenium nanoparticles in the presence of polysaccharides. Mater Lett 58:2590–2594. https://doi.org/10.1016/j.matlet.2004.03.031